

## CFD modeling and experimental study of pulse flow in a hollow fiber membrane for water filtration

Zaifeng Shi<sup>a,b,\*</sup>, Chen Li<sup>a,b</sup>, Ting Peng<sup>a,b</sup>, Xiaowei Qiao<sup>a,b</sup>, Qiang Lin<sup>a,b,\*</sup>, Linhua Zhu<sup>a,b</sup>, Xianghui Wang<sup>a,b</sup>, Xuyan Li<sup>a</sup>, Mei Zhang<sup>a</sup>

<sup>a</sup>Key Laboratory of Water Pollution Treatment & Resource Reuse, Hainan Province, China, Tel. +86 13086013920, email: zaifengshi@163.com (Z. Shi), Tel. +86 18245286056, email: 1196159358@qq.com (C. Li), Tel. +86 15968660529, email: 18389946479@163.com (T. Peng), Tel. +86 13519807171, email: 47717723@qq.com (X. Qiao), Tel. +86 13807654689, email: lingqiangroup@163.com (Q. Lin), Tel. +86 18389381716, email: zhulinhua1981@163.com (L. Zhu), Tel. +86 15607619609, email: god820403@163.com (X. Wang), Tel. +86 18789559673, email: 820308986@qq.com (X. Li), Tel. +86 15595694291, email: 649098897@qq.com (M. Zhang)

<sup>b</sup>College of Chemistry and Chemical Engineering, Hainan Normal University, Hainan Province, China

Received 8 December 2015; Accepted 6 December 2016

### ABSTRACT

In this paper, two kinds of pulse feed including sinusoidal pulse flow (SPF) and intermittent pulse flow (IPF) were applied at the entrance of the ultrafiltration (UF) module with hollow fiber membrane, which were more effective for flux enhancement. As compared to compared to continuous flow at the same average velocity, the improvement of permeation flux could reach up to 80% for SPF and 44% for IPF, respectively. The mechanism of pulse feeding on flux enhancement was explored and a comprehensive analysis of the shear stress distribution along the membrane surface has been performed by a three-dimensional computational fluid dynamics (3D CFD) model. Additionally, comparison of pressure drop between pulse feed and steady flow was done to evaluate energy consumption. Results indicated that sinusoidal pulse flow (SPF) led to higher shear force and higher efficiency in UF process than IPF, which is consistent with experiments.

*Keywords:* Hollow fiber ultrafiltration membrane; Pulse feed; Shear force; 3D CFD

### 1. Introduction

Due to low energy consumption, easy operation, high removal efficiency of bacteria and micro-organisms, ultrafiltration (UF) has been widely used in different fields such as drinking water purification, wastewater treatment, clarification, and separation in pharmaceutical industry, biotechnology and biomedicine [1,2]. However, like other membrane processes, membrane fouling is one of the main technical challenges impeding the industrialization of UF process caused by the concentration polarization and particle deposition [3], which leads to the blockage of membrane

pores [4] or the formation of a cake layer on the membrane surface [5], and thus an undesirable dramatic decline of permeate flux.

A large amount of methods have been proposed to alleviate membrane fouling and enhance the process performance [6]. In recent studies, the introduction of turbulence promoter into the membrane filtration, including mixers [7], baffles [8], and spacers [9], has been investigated experimentally and numerically [10,11]. Although it exhibits the excellent positive enhancement to membrane filtration process, turbulence promoter may induce higher pressure drop along the channel with lots of unnecessary energy consumption [6,12,13]. Air sparging can be used as a feasible fouling control or flux enhancement method to maintain the filtration process with good productivity [14]. Air is needed

\*Corresponding author.

to be pumped into the feed stream to form a gas/liquid two-phase flow. However, compressed air has the potential to cause membrane damage and rewetting [15]. Owing to the recent improvements in the transducer system [16], the ultrasound has been used to reduce membrane fouling in UF process, which can give significant improvement in permeate flux at a low frequency of ultrasound irradiation [17,18]. But the disadvantage of ultrasound is the high cost including both the capital cost and the installment of transducers for the ultrasonic system.

In order to overcome the potentially high costs, researchers have attempted to find more convenient and low-energy methods to improve the flux recovery. Recently, pulsating flow is widely recognized as a safer and higher efficiency method for membrane fouling control [6,19]. By using pulsating flow at the entrance, shear stress will be increased adjacent to the membrane surface, resulting in a lift force preventing particles deposition on the membrane surface. And the boundary layer will be disrupted without any damage of the membrane surface. Also, there are quite big differential pressures between two neighboring pulses, causing backflow and shear stress sweeping particles from the membrane surface and membrane pore simultaneously.

Wilharm [20] investigated the effects of the pulse amplitude and duration on the permeate flux in UF process. The results showed that not only transmembrane pressure pulsing may improve the flux but also the induced backward flow could carry the sediments out away from the membrane pore. Similar results were obtained in Sanjeev's study [21], in which rapid back pulsing was investigated to reduce membrane fouling. Gironès i Nogué et al. [22] proved that pressure pulsing could alleviate the polarization phenomena. Hwang et al. [23] looked into a pulse feeding method that increased the filtration flux by 25%, which had great potential to significantly mitigate membrane pore blocking.

As a practical technique computational Fluid Dynamics (CFD) has been used to simulate fluid hydrodynamics in the membrane process [24–27]. CFD can vividly describe the flow characteristics under different types of conditions such as pulse feed or turbulent flow [28–31] and attentions are being paid on the applications of CFD technology into the membrane process. F. Li et al. [32] used 3D CFD simulation for the spiral wound membrane to simulate mass transfer and evaluate the related coefficients. They found the optimum ratio of channel height over spacer length to attain the largest mass transfer efficiency by numerical simulation and experimental validation [33]. The similar simulation for tubular membrane in cross flow filtration was described by K. Damak et al. [34]. In addition, CFD simulation was also applied to predict the concentration polarization profile, mass transfer coefficient and wall shear stress in narrow membrane channel [35]. The simulation results showed that concentration polarization phenomena could be reduced by increasing feed Reynolds number, and the low wall shear stress also contributed to the formation of the concentration polarization layer. It is consistent with A. Pak's study [36] in which the laminar flow in porous tubes was simulated numerically using the CFD techniques by solving Navier-Stokes, Darcy's law and mass transfer equation. Jalilvand et al. [19] focused on using a 3D CFD model to simulate the hydrodynamics

in a flat sheet microfiltration module. It was found that the highest shear force was obtained at the entrance region and pulsatile flow led to higher flux in comparison with continuous flow.

Although few experimental investigations and CFD analysis on pulsatile flow have been carried out to relieve membrane fouling and enhance the performance of membrane processes [37]. No systematical investigation on the operation parameters of the pulse flow (e.g., pulse magnitude and frequency) in the hollow fiber membrane module was reported. The purpose of this work was to investigate the effects of two kinds of pulse feed, including sinusoidal pulse flow (SPF) and intermittent pulse flow (IPF), on UF process using hollow fiber membrane for treating the synthetic wastewater. In order to further understand the reasons of pulse flow in improving membrane flux, a 3D CFD simulation was built in FLUENT 14.0 to simulate UF process and fluid flow, and shear force near the membrane wall was calculated. Effects of pulse frequency and magnitude on the shear force in UF process were systematically discussed. Furthermore, comparison of pressure drop at different flow patterns were also done to assess the energy consumption, which would provided a useful guide for the application of pulse feed in UF process.

## 2. Theory

### 2.1. Geometric structure and mesh generation

The 3D geometric structures of the membrane module were created by commercial software Gambit 2.4.6. The main parameters of membrane module and hollow fiber membrane are shown in Table 1. In the module, ten PVC membrane fibers were packed. However, single of fiber membrane was considered in the simulation. It is to discuss shear force near membrane wall with different flow pattern. Hollow fibers are modeled as rigid elements because fibers are tightly potted in the module. This is caused by the centrifugal force applied on fibers during epoxy potting; therefore, sway of fibers is neglected [38]. The module and fiber were divided into ten pieces by establishing faces so that the shear force could be calculated near the membrane wall. The creation of the hollow fiber membrane is shown in Fig. 1.

The cooper of meshing method was adopted because the diameter of the fiber was too smaller compared to the module. For the near membrane wall, the boundary layer mesh grid was adopted on the membrane wall due to the large velocity gradient. The height of the first grid layer was  $10^{-4}$  m, and a total of ten layers. Then, hexahedral mesh was used. On the other hand, for inlet and outlet port, a

Table 1  
The main dimensions parameters of membrane module and membrane

	Length	Outer diameter	Inner diameter	Outlet diameter	Porosity
Module	300 mm	φ 30 mm	–	φ 5 mm	–
PVC fiber	280 mm	φ 1.6 mm	φ 1.3 mm	–	85%

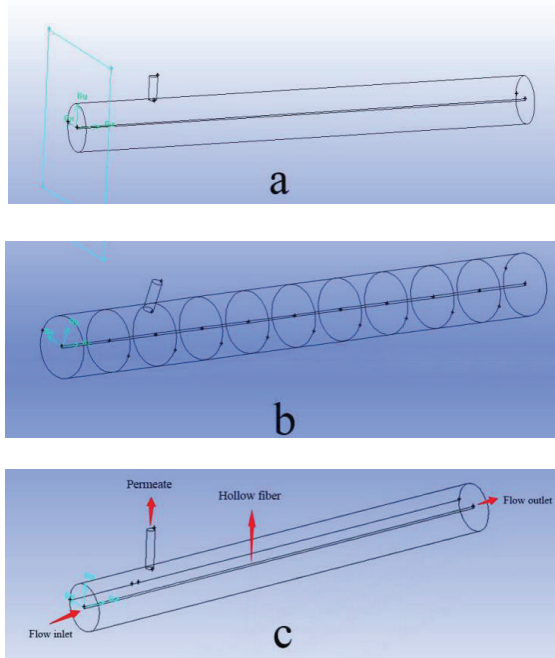


Fig. 1. The creation of hollow fiber membrane used in the simulations (a) the geometric model of hollow fiber membrane; (b) the membrane module was divided into ten sections; (c) the boundary condition of UF process.

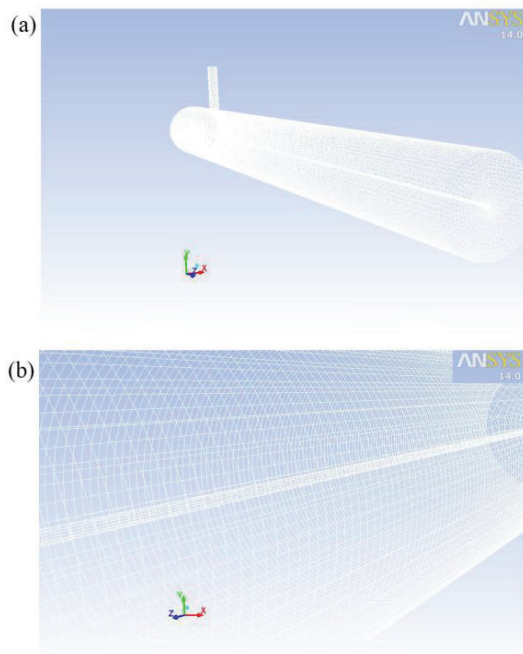


Fig. 2. The meshed geometry (a) the membrane module; (b) the partial membrane module.

normal quadratic mesh was used. Grids were refined near the membrane surface as shown in Fig. 2. It was found that the number of grids was 35 w and the quality of the grids showed good.

### 2.2. Governing equations and boundary condition

With the geometries structured, CFD simulations were carried out according to the governing transport equations. In the simulation, it is assumed that the fluid is incompressible and isothermal. Also, the density  $\rho$  and dynamic viscosity  $\mu$  of the mixed feed solution were calculated based on volume-weighted-mixing-law and mass-weighted-mixing-law, respectively. The hydrodynamics in a cross-flow hollow fiber UF process can be discretized by solving the governing equations including mass balance and Navier-Stokes equations in cylindrical coordinate system, as shown in the following:

The continuity equations:

$$\frac{\delta \rho}{\delta t} + \frac{\delta(r\rho v)}{r\rho r} + \frac{\delta(\rho v_\theta)}{r\delta\theta} + \frac{\delta(\rho v_z)}{\delta z} = 0 \quad (1)$$

Because  $\rho$  is constant,  $\frac{\delta \rho}{\delta t} = 0$ ,

$$\frac{\delta(rv_r)}{r\delta r} + \frac{\delta v_\theta}{r\delta\theta} + \frac{\delta v_z}{\delta z} = 0 \quad (2)$$

And N-S equation in r-direction:

$$\rho \left( \frac{\delta v_r}{\delta t} + v_r \frac{\delta v_r}{\delta r} + \frac{v_\theta}{r} \frac{\delta v_r}{\delta\theta} - \frac{v_\theta^2}{r} + v_z \frac{\delta v_r}{\delta z} \right) = \rho F_r - \frac{\delta P}{\delta r} + \mu \left\{ \frac{\delta}{\delta r} \left[ \frac{1}{r} \frac{\delta}{\delta r} (rv_r) \right] + \frac{1}{r^2} \frac{\delta^2 v_r}{\delta\theta^2} - \frac{2}{r^2} \frac{\delta v_r}{\delta\theta} + \frac{\delta^2 v_r}{\delta z^2} \right\} \quad (3)$$

N-S equation in  $\theta$ -direction:

$$\rho \left( \frac{\delta v_\theta}{\delta t} + v_r \frac{\delta v_\theta}{\delta r} + \frac{v_\theta}{r} \frac{\delta v_\theta}{\delta\theta} - \frac{v_\theta^2}{r} + v_z \frac{\delta v_\theta}{\delta z} \right) = \rho F_\theta - \frac{1}{r} \frac{\delta P}{\delta r} + \mu \left\{ \frac{\delta}{\delta r} \left[ \frac{1}{r} \frac{\delta}{\delta r} (rv_\theta) \right] + \frac{1}{r^2} \frac{\delta^2 v_\theta}{\delta\theta^2} - \frac{2}{r^2} \frac{\delta v_r}{\delta\theta} + \frac{\delta^2 v_\theta}{\delta z^2} \right\} \quad (4)$$

N-S equation in Z-direction:

$$\rho \left( \frac{\delta v_z}{\delta t} + v_r \frac{\delta v_z}{\delta r} + \frac{v_\theta}{r} \frac{\delta v_z}{\delta\theta} + v_z \frac{\delta v_z}{\delta z} \right) = \rho F_z - \frac{\delta P}{\delta r} + \mu \left\{ \frac{1}{r} \frac{\delta}{\delta r} \left( r \frac{\delta v_z}{\delta r} \right) + \frac{1}{r^2} \frac{\delta^2 v_z}{\delta\theta^2} + \frac{\delta^2 v_\theta}{\delta z^2} \right\} \quad (5)$$

where  $F_r, F_\theta, F_z$  are the drag force along the direction of  $r, \theta, z$ , respectively, (N).  $v_r$  is the velocity of  $r$  component of,  $v_\theta$  is the velocity of  $\theta$  component, and  $v_z$  is the velocity of  $z$  component, ( $m s^{-1}$ ).  $P$  is the pressure, (Pa) and  $\rho$  is the density of fluid, ( $g cm^{-3}$ ).

In the simulation, a laminar model is used to simulate hydrodynamic situation in the module under laminar operating conditions ( $Re < 2000$ ) and a realizable  $k-\epsilon$  [33] model

is applied under turbulent conditions ( $Re > 2000$ ) induced by the pulse flow, where  $k$  is the turbulence kinetic energy, ( $\text{m}^2/\text{s}^2$ ) and  $\varepsilon$  is the turbulence dissipation rate, ( $\text{m}^2/\text{s}^3$ ). The transport equations can be expressed as:

$$\frac{\delta(\rho k)}{\delta t} + \Delta \rho \bar{u} k = \Delta \left[ \left( \mu k + \frac{\mu_{eff}}{\sigma_k} \right) \Delta k \right] + \mu_{eff} S^2 - \rho \varepsilon \quad (6)$$

$$\frac{\delta(\rho \varepsilon)}{\delta t} + \Delta \rho \bar{u} \varepsilon = \Delta \left[ \left( \mu \varepsilon + \frac{\mu_{eff}}{\sigma_\varepsilon} \right) \Delta \varepsilon \right] + C_1 S - \rho \varepsilon - C_2 \frac{\rho \varepsilon^2}{k + \sqrt{\nu \varepsilon}} \quad (7)$$

where

$$\mu_{eff} = C_\mu \rho \frac{k^2}{\varepsilon}$$

$$S = \sqrt{2S_{ij}S_{ij}}$$

$$S_{ij} = \frac{1}{2} \left( \frac{\partial u_i}{\partial x_j} + \frac{\partial u_j}{\partial x_i} \right)$$

$$C_1 = \max \left[ 0.43 \frac{\eta}{\eta + 5} \right]$$

$$\eta = S \frac{k}{\varepsilon}$$

$$C_2 = 1.9$$

$$\sigma_k = 1.0$$

$$\sigma_\varepsilon = 1.2$$

Boundary conditions are quite important for numerical computing. In this study, two different pulse feeds including SPF and IPF were carried out. The expressions of inlet velocity are shown as the following:

For sinusoidal pulse flow:

$$V = A + A \sin \left( \frac{2\pi}{T} t + \gamma_0 \right) \quad (8)$$

For intermittent pulse flow:

$$V = \begin{cases} A & 0 < t < \frac{T}{2} \\ 0 & \frac{T}{2} < t < T \end{cases} \quad (9)$$

where  $A$  is pulse magnitude, ( $\text{m/s}$ ),  $T$  is pulse period, ( $\text{s}$ ) and  $\gamma_0$  is the initial phase. The inlet velocity was defined in the user defined function (UDF). The corresponding profiles of shear stress under the two types of pulse flow are illustrated in Fig. 3. The shear profiles arise from a change of velocity, which was controlled by a programmable pulse controller. At the outlet port, constant gauge pressure was set as 80 kPa.

### 2.3. Numerical method

With the 3D CFD model, transient is used to simulate the pulse system by first order implicit. The scheme based on segregated solver, second order upwind discretization and SIMPLE algorithm were chosen. A second order upwind scheme was chosen for momentum, the simulation was based on the mixture model and the standard  $k-\varepsilon$  was employed to describe the turbulent fluid flow in the modeling. With the turbulent dissipation ( $\varepsilon$ ) introduced using the first order upwind. The intensity and hydraulic diameter were chosen to set the parameter of turbulence. As default absolute convergence criteria,  $10^{-3}$  was used for the solution variables.

## 3. Experimental

### 3.1. Feed preparation and membrane properties

The stock solution of humic acid (HA) was prepared by adding 1 g of HA to 250 ml of 0.01 mol/l sodium hydroxide (NaOH) solution with magnetically stirring 12 h to make HA fully dissolved.

The hollow-fiber UF membrane is made of Polyvinyl Chloride (PVC) (Litree Co., China). Because there are eth-

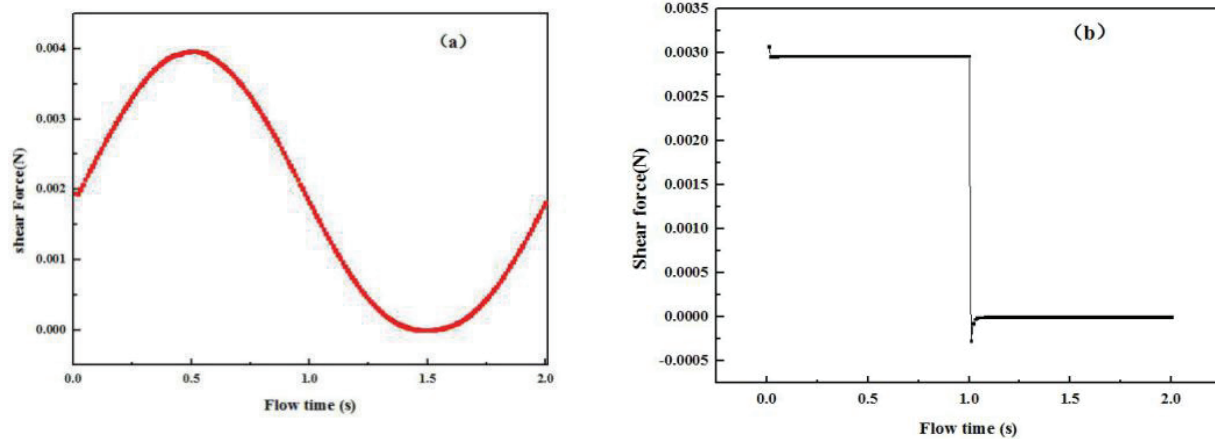


Fig. 3. Shear profiles at the inlet of the membrane module (a) for SPF; (b) for IPF.

anol and glycerol as protective liquid in the membrane fibers, the membranes must be washed repeatedly with distilled water before using.

### 3.2. Scanning electron microscope (SEM) analysis

Hollow fiber UF membrane used at different experimental conditions were freeze-dried at  $-60^{\circ}$  for 24 h, and a small piece of membrane sample was air-dried and sputter coated with gold (Au) before being examined at 10 kV accelerating voltage for SEM analysis (JSM-7100F, JEOL, Japan).

### 3.3. Experimental setup and procedures

The experimental setup used in this study is shown in Fig. 4. The feed was pumped from feed tank to the hollow fiber membrane and the retentate was cycled to the reservoir. The cross-flow velocity was recorded and controlled by the rotameter. A pulse controller was installed at the entrance of the membrane module to control the outputs of pulse frequency and magnitude. The filtrate was collected into a vessel and weighed using the electronic balance. The feed was stirred uniformly using a magnetic mixer with temperature maintained at  $20^{\circ}$ . The pressure was adjusted using the outlet valve coupled with two pressure gauges installed on the two sides of the membrane module. Furthermore, the transmembrane pressure (TMP) of the system was recorded by the average value of the inlet and outlet pressure.

## 4. Result and discussion

### 4.1. Experimental results

#### 4.1.1. Effect of flow pattern on permeate flux

Initially, UF experiments were performed to ascertain the unsteady flow at the inlet. The unsteady flows (SPF and IPF) were both controlled at the same value of average velocity of  $0.15 \text{ m s}^{-1}$ . According to Fig. 5, the permeate fluxes decreased

quickly first and then the reduction became gentle with filtration time. Filtration was terminated when a constant flux was obtained for each test. It could be observed that pulse feed could significantly improve the fluxes. Specifically, the flux improvement by SPF was the most effective, for 80% was improved. IPF was found to contribute to slightly improvement in flux, for 44% was enhanced. Furthermore, a further increase of the steady velocity to  $0.3 \text{ m s}^{-1}$  also showed a lower permeates flux compared to pulse flows. This demonstrates the effectiveness of using pulse flow in enhancing the filtration performance. It can be deduced that intense velocity fluctuation induced by the pulsatile flow led to the vibration of hollow fiber membrane and an improvement of the shear stress adjacent to the membrane wall, which is beneficial to mitigate the fouling formation on the membrane surface or in the membrane pores.

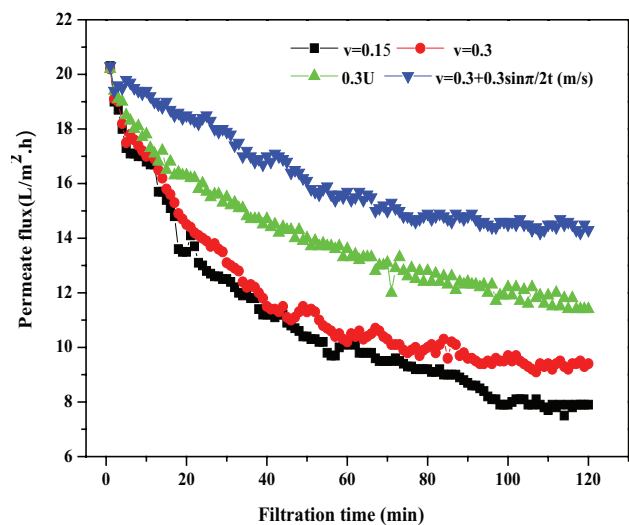


Fig. 5. Permeate flux vs. filtration time under steady and unsteady flow (sinusoidal and intermittent pulse flows) at the inlet of UF module ( $C = 1.5 \text{ g/l}$ ,  $TMP = 80 \text{ kPa}$ ).

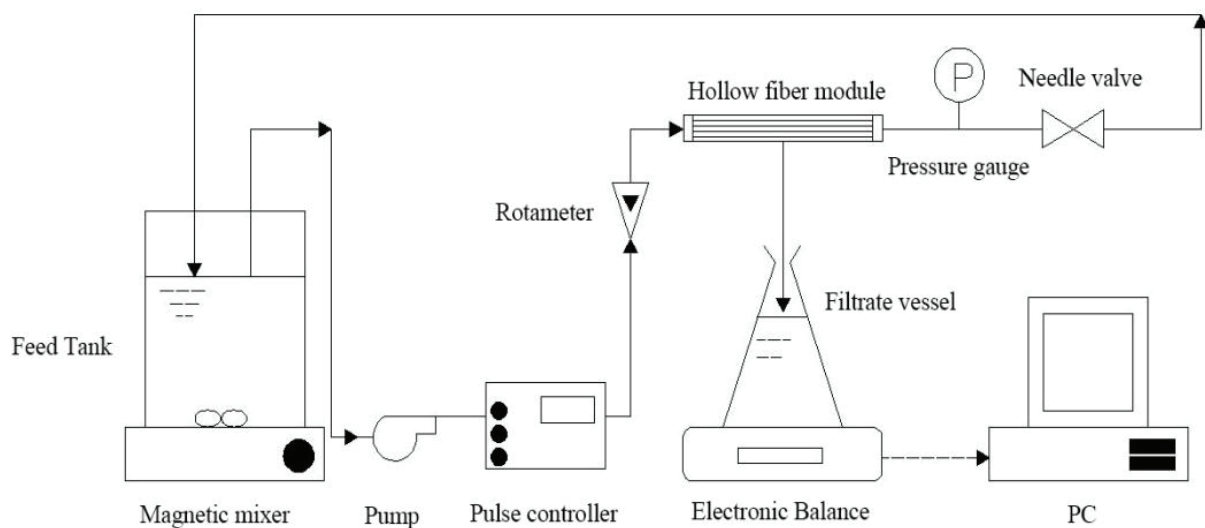


Fig. 4. Set-up diagram of UF process.

#### 4.1.2. Morphology analysis

The samples of new and fouled membranes were observed with SEM to demonstrate the changes in morphology with steady and unsteady flows. As displayed in Fig. 6, the surface of new membrane was rather smooth and clear. By contrast, the surfaces of the fouled membranes were obviously covered by a fouling layer after filtration (Fig. 6b–d). However, the density of the layer formed with different types of feed was different. The morphology of the membrane surfaces fouled by pulse feed (Fig. 6c and 6d) was more apparently uniform than that by continuous flow (Fig. 6b). Therefore the introduction of pulse feed had a notable change, having thinner fouling layers. Also, the degree of pollution with SPF was slightly lighter as compared with that of IPF, indicating SPF was better IPF for the eliminate the fouling.

#### 4.2. Numerical results

In order to explore the intrinsic mechanism of flux improvement with pulse feed, 3D CFD simulation of fluid flow was implemented. The shear force adjacent to the membrane wall was calculated by integrating shear stress along the membrane length on the basis of Eqs. (10)–(12). The basic definition for shear stress distribution is as follows:

$$\tau_{zz} = \mu \left( 2 \frac{\delta u}{\delta z} - \frac{2}{3} \nabla \cdot \vec{v} \right) = \frac{2}{3} \mu \left( 2 \frac{\delta u}{\delta z} - \frac{\delta v_r}{r \delta r} - \frac{\delta v_\theta}{r \delta \theta} \right) \quad (10)$$

$$\tau_{rz} = \mu \left( \frac{\delta v_r}{\delta z} + \frac{\delta u}{\delta r} \right) \quad (11)$$

$$\tau_{\theta z} = \mu \left( \frac{\delta v_\theta}{\delta z} + \frac{\delta u}{r \delta \theta} \right) \quad (12)$$

$$F_z = - \left( \int_0^{0.3} \int_0^{2\pi} \tau_{rz} r d\theta dz + \int_0^{0.015} \int_0^{2\pi} \tau_{zz} r d\theta dr + \int_0^{2\pi} \int_0^{0.015} \tau_{\theta z} dr d\theta \right)$$

where  $\tau$  is shear stress,  $\mu$  is the fluid's viscosity,  $F_z$  is the shear force along the fluid flow direction ( $z$ ) through membrane channel dimensions, from 0 to 0.3 m in  $z$  direction, 0 to 0.015 m in  $r$  direction, and 0 to  $2\pi$  in  $\theta$  direction.

##### 4.2.1. Effect of flow pattern on shear force

The calculated shear force along the flow direction under different flow patterns is plotted in Fig. 7. A descending trend of the shear force curve is observed along the flow direction, which is in consistent with

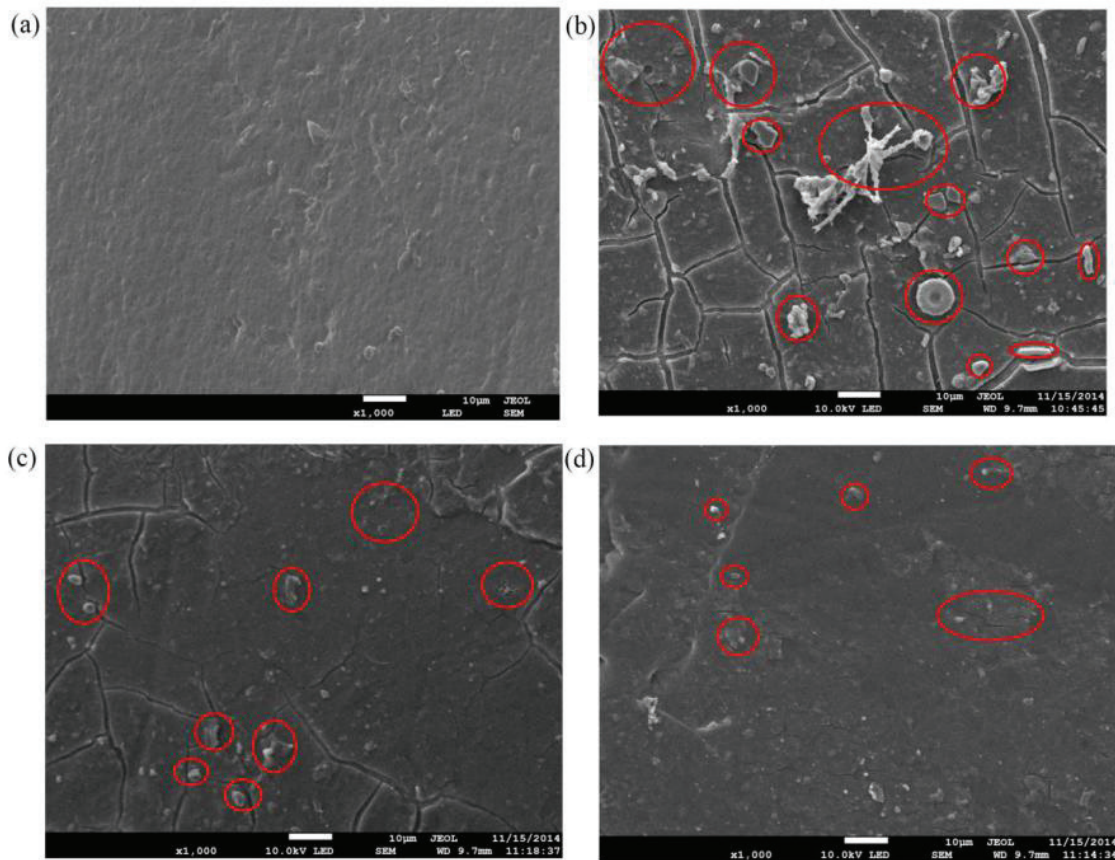


Fig. 6. Images of PVC hollow fiber membrane (a) new membrane surface; (b) membrane surface without pulse flow in UF process; (c) membrane surface with IPF in UF process; (d) membrane surface with SPF in UF process ( $C = 1.5$  g/L,  $TMP = 80$  kPa, the same average velocity of 0.15 m/s).

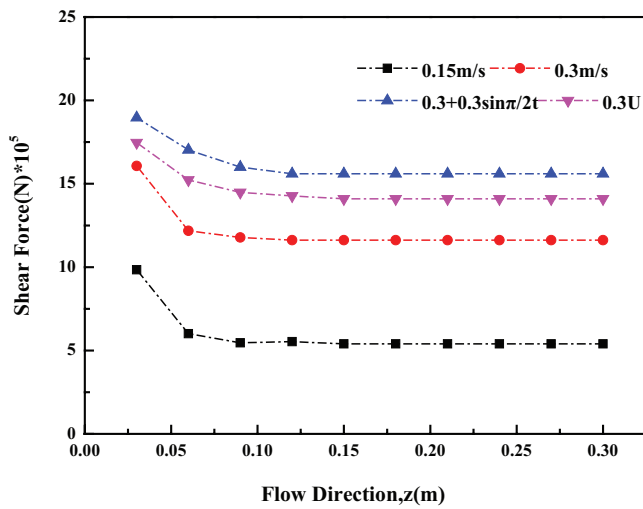


Fig. 7. The shear force along the flow direction under different flow patterns ( $C = 1.5 \text{ g/l}$   $TMP = 80\text{kPa}$ ).

the previous studies [30]. As expected, the shear stress increases with increasing the velocity (from  $0.15$  to  $0.3 \text{ m s}^{-1}$ ) [39,40]. It can be seen that, the shear forces of pulsatile flow were enhanced nearly two fold than that of steady flow with the same average velocity ( $v = 0.15 \text{ m/s}$ ) at the inlet port. It may be explain that pulse feed could significantly improve UF process. In comparison of the two different types of pulse flow, the shear force of SPF was slightly higher than that of IPF at the inlet. And the shear force of SPF at the exit was equal to that of IPF at the inlet port. Additionally, the results also indicate that the shear force at the steady flow velocity ( $v = 0.3 \text{ m s}^{-1}$ ) is even smaller than that of pulsatile flow with the average velocity of  $0.15 \text{ m s}^{-1}$ . Thereby, the enhancement of permeation (Fig. 5) with pulse feed may attribute to the improvement of shear stress near membrane surface. The fluctuations of inlet velocity not only cause back-flow but also alleviate the cake compression on the membrane surface or in the membrane pores [41].

#### 4.3. Effects of the operation parameters

It is well-known that the magnitude and period are the most important factors influencing the performance of filtration process [19]. In this section, the influences of magnitude and frequency of pulse feed were systematically studied.

##### 4.3.1. Pulse periods

Fig. 8a and 8b show the variation of shear force along the flow direction with SPF and IPF, respectively. The pulse period range from  $0.1$  to  $0.8 \text{ s}$  was investigated by 3D CFD. Basically, low pulse periods resulted in shear force increasing independence of the flow types applied. However, the response of shear force to increasing pulse periods were obviously affected by the pulse types, which is depicted as Fig. 8c. In the case of SPF, pulse periods under  $0.1$  to  $0.5 \text{ s}$  resulted in dramatically decline with the

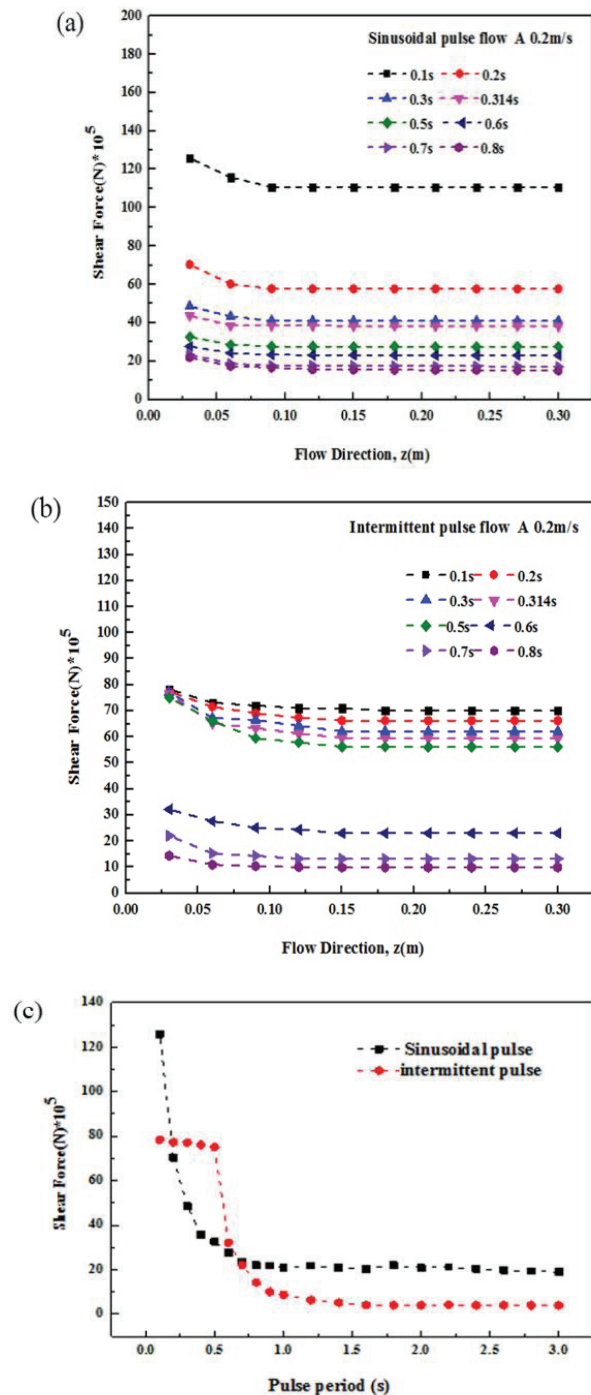


Fig. 8. Effect of pulse period on shear force (a) sinusoidal pulse flow; (b) intermittent pulse; (c) pulse period vs. shear force at the inlet with two different pulses feed ( $C = 1.5 \text{ g/l}$   $TMP = 80\text{kPa}$ ).

rise of pulse periods. While that of shear force increased gently with pulse period over  $0.5 \text{ s}$ . For IPF, shear force remained slightly decrease with periods ranging from  $0.1$  to  $0.5 \text{ s}$  and declined sharply when period was added from  $0.5$  to  $0.8 \text{ s}$ , and then reached a plateau when period was higher than  $1.0 \text{ s}$ . Therefore, there existed the optima

pulse period of 0.5 s with the IPF. Combining the equation shown in (8) and (9), the possible reason was that various pulse period would lead to the intense velocity fluctuation. The lower pulse period increased the fluctuation intensity of the flow rates; meanwhile the vibration of module was frequently produced. Additionally, if the pulse frequency was blindly increased, it would be at the expense of more energy consumption, which would be presented in section 4.4 of this study.

The influence of pulse magnitudes ( $A$ ) on shear force was discussed. In Fig. 9a and 9b, there is an increase tendency of shear force with the growth of pulse magnitude, no matter using SPF or IPF. From Fig. 9c, the differences between SPF and IPF are listed. At a comparatively low pulse magnitude of 0.1–0.2 m/s, the shear force between SPF and IPF indicated no obvious differences. The main reason may be that the feed velocity would be nearly equal under the condition of low pulse magnitude on basis of Eqns. (8) and (9). With the increasing pulse magnitude, the shear force presented an increasing trend and kept rising significantly, and when it came to 0.8 m/s, the shear force of SPF reached 260 (unit:  $N/10^5$ ) and that of IPF was only 160. The reason may be contributed to the formation of vortex with high velocity, that resulting in more cake removal and higher filtration flux [42]. As a result, shear stress near the membrane wall that acted as an important factor affecting particle depositing had a more significant change with SPF. Generally speaking, the frequency and magnitude with pulse feed bring about the fluctuation tendency of inlet velocity, which can greatly disrupt the development of boundary layer and reduce the particle deposition on the membrane surface [43].

#### 4.4. Pressure drop

The pressure drop distribution at the central of membrane tube was obtained by CFD simulations under controlled conditions including pulse frequency and magnitude, and the results are shown in Tables 2 and 3. Pressure drop with steady flow was displayed in Table 4. With pulse magnitude fixed at 0.2 m/s, the pressure drop decreased gradually accompanying with the increasing pulse periods whichever method was utilized. The highest pressure drop reached 992.99 Pa under pulse period of 0.1 s. It was apparently that there were discriminately differences with periods over 0.5 s. Comparison of pressure drop with the same pulse periods of 0.7 s was listed in Table 3, which gave a rising trend of pressure drop with the continuous growth of pulse magnitude. The pressure drop was higher than that of steady flow at the same inlet velocity, which was owing to the impulsive disturbance. Although, pulsatile flow would generate higher pressure drop and more energy loss, in the long run, the pulse flow with appropriate pulse parameters may be a right decision. The reason may be that pulse feed was accompanied with higher shear force and low cake formation, which could postpone the membrane fouling. Low shear force always caused by steady flow may result in higher fouling and cake layer formation, ultimately the performance of membrane was decreased and high pressure was demanded to maintain fluxes. Accordingly, pulsatile flow can be definitely an efficient way to enhance membrane filtration.

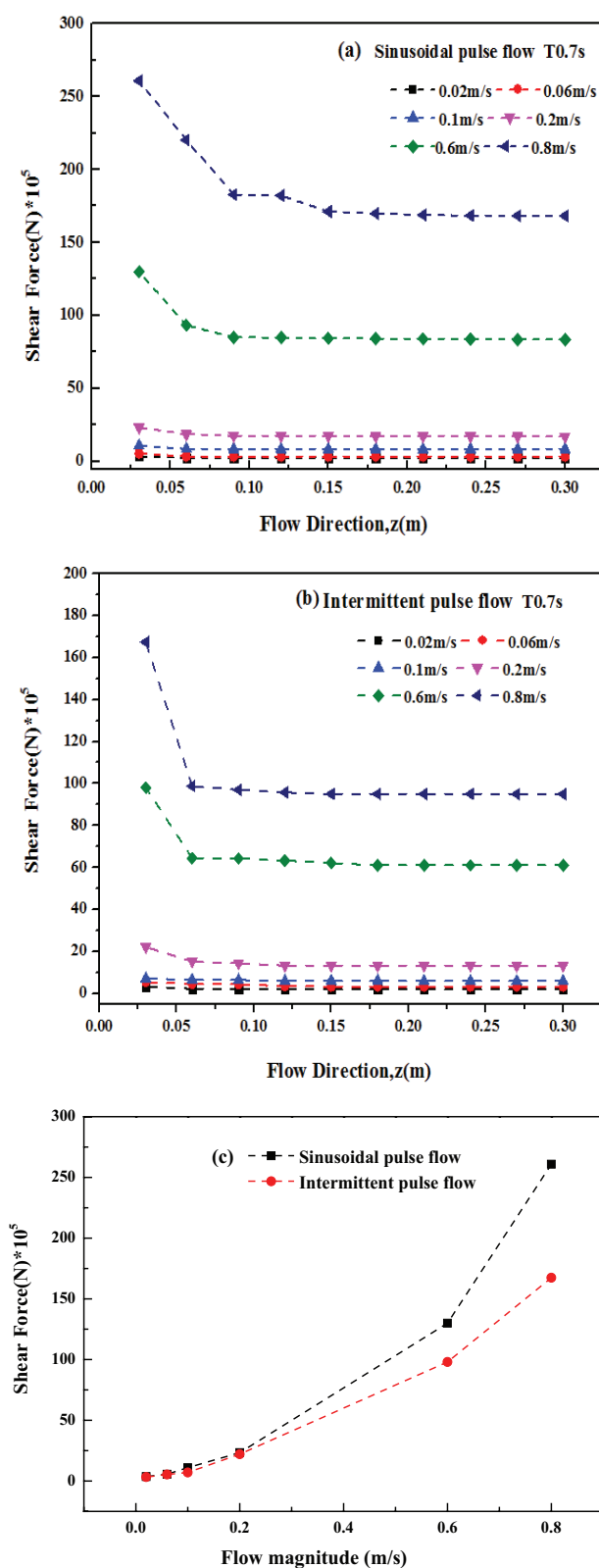


Fig. 9. Effect of pulse magnitude on shear force with different flow patterns (a) sinusoidal pulse; (b) intermittent pulse; (c) pulse magnitude vs. shear force at the inlet with two different pulses feed ( $C = 1.5\text{g/l}$ ,  $TMP = 80\text{ kPa}$ ).

Table 2  
Comparison of pressure drop between SPF and IPF with the same pulse magnitude of 0.2 m/s ( $C = 1.5$  g/L outlet pressure: 80 kPa)

Parameters	Pressure drop (unit: Pa) SPF	Pressure drop (unit: Pa) IPF
T 0.1 s	992.99	872.54
T 0.3 s	852.47	805.63
T 0.5 s	685.79	512.74
T 0.7 s	405.76	297.63
T1.0 s	203.45	118.74

Table 3  
Comparison of pressure drop between SPF and IPF with the same pulse periods of 0.7s ( $C = 1.5$  g/L outlet pressure: 80 kPa)

Parameters	Pressure drop (unit: Pa) SPF	Pressure drop (unit: Pa) IPF
A 0.1 m/s	104.32	116.54
A 0.3 m/s	405.7	407.63
A 0.5 m/s	652.32	486.79
A 0.7 m/s	1015.67	857.63
A 1.0 m/s	1543.24	1325.47

Table 4  
Pressure drop with steady flow ( $C = 1.5$  g/L outlet pressure: 80 kPa)

Parameters	Pressure drop (unit: Pa) SPF
0.05 m/s	94.62
0.15 m/s	367.54
0.25 m/s	425.63
0.35 m/s	612.36
1.0 m/s	975.19

## 5. Conclusions

Using pulse feed such as SPF and IPF has been proven effective in enhancing flux. The study has revealed that the flux enhancement were improved 80 and 44% under the same condition with SPF and IPF, respectively. Both SPF and IPF gave similar results in terms of flux enhancement and energy consumption, with the former slightly better.

The use of 3D CFD in hollow fiber made it possible to consider the shear force and the pressure drop, which could fully explain the improvement of flux and energy loss. Accordingly, the effects of pulse period and magnitude were comprehensively discussed. The response of shear force to increasing pulse periods and magnitude were obviously affected by the pulse types. The data showed that with the increasing pulse magnitude and frequency, the pressure drop augmented sharply. When the pulse magnitude was  $1.0 \text{ m s}^{-1}$  and period was fixed at 0.7 s, pressure

drop reached 1543.24 Pa for SPF and 1325.47 Pa for IPF, nearly twice in comparison with steady flow at the same velocity of  $1.0 \text{ m s}^{-1}$ . However, when the average velocity was  $0.05 \text{ m s}^{-1}$ , there were slightly differences which could be negligible between pulse feed and continues flow. Therefore, pulse feed can be used to mitigate membrane fouling and enhance membrane performance with high efficient.

## Acknowledgements

Thanks are given to the Department of Science & Technology of Hainan Province, P.R.China for program fund (ZDKJ2016022-02). Also, PhD Guizi Chen from Nanyang Technological University (Singapore) and Prof. Wei Sun from Hainan Normal University (China) provided lots of help and suggestions during the paper preparation. So, authors are grateful to them all. The author would like to acknowledge the Education Department of Hainan province (Postgraduate technology innovation project, Hys2014 - 56) and Hainan Normal University (Students Innovation Training, cxcyxj2014010) for the financial supports

## Nomenclature

$\rho$	— density ( $\text{kg m}^{-3}$ )
$\mu$	— viscosity (Pa s)
$r, \theta, z$	— cylindrical coordinate (m)
$v_r, v_\theta, v_z$	— mean velocity component ( $\text{m s}^{-1}$ )
$F_r, F_\theta, F_z$	— the drag force along the direction of $r, \theta, z$ .
$P$	— pressure (Pa)
$k$	— turbulence kinetic energy ( $\text{m}^2/\text{s}^2$ )
$\varepsilon$	— turbulence dissipation rate ( $\text{m}^2/\text{s}^3$ )
$A$	— pulse magnitude (m/s)
$T$	— pulse period
$\gamma_0$	— initial phase
$\tau$	— shear stress
$\mu_{eff}$	— eddy viscosity (pa-s)
$C_1, \sigma_k, \sigma_\varepsilon, C_1$	— adjustable constants

## References

- [1] Z.F. Cui, S. Chang, A.G. Fane, The use of gas bubbling to enhance membrane processes, *J. Membr. Sci.*, 221 (2003) 1–35.
- [2] W. Gao, H. Liang, J. Ma, M. Han, Z.L. Chen, Z.S. Han, G.B. Li, Membrane fouling control in ultrafiltration technology for drinking water production: A review, *Desalination*, 272 (2011) 1–8.
- [3] D. Jermann, W. Pronk, R. Kägi, M. Halbeisen, M. Boller, Influence of interactions between NOM and particles on UF fouling mechanisms, *Water Res.*, 42 (2008) 3870–3878.
- [4] B. Wojciech, E. Celińska, R. Dembczyński, D. Szymanowska, M. Nowacka, T. Jesionowski, W. Grajek, Cross-flow microfiltration of fermentation broth containing native corn starch, *J. Membr. Sci.*, 427 (2013) 118–128.
- [5] J. Shin, K. Kim, J. Kim, S. Lee, Development of a numerical model for cake layer formation on a membrane, *Desalination*, 309 (2013) 213–221.
- [6] G.A. Fimbres-Weihs, D.E. Wiley, Review of 3D CFD modeling of flow and mass transfer in narrow spacer-filled channels in membrane modules, *Chem. Eng. Process*, 49 (2010) 759–781.
- [7] S. Popović, D. Jovičević, M. Muhadinović, S. Milanović, M.N. Tekić, Intensification of microfiltration using a blade-type turbulence promoter, *J. Membr. Sci.*, 425–426 (2013) 113–120.

- [8] Y.F. Liu, G.H. He, X.D. Liu, G.K. Xiao, B.J. Li, CFD simulations of turbulent flow in baffle-filled membrane tubes, *Sep. Purif. Technol.*, 67 (2009) 14–20.
- [9] T. Wang, Z.G. Zhang, X.J. Ren, L. Qin, D.J. Zheng, J.D. Li, Direct observation of single- and two- phase flows in spacer filled membrane modules, *Sep. Purif. Technol.*, 125 (2014) 275–283.
- [10] Y.F. Liu, G.H. He, L.H. Ding, H. Dou, J. Ju, B.J. Li, Experimental and CFD studies on the performance of microfiltration enhanced by a turbulence promoter, *Chinese J. Chem. Eng.*, 20 (2012) 617–624.
- [11] X. Yang, H. Yu, R. Wang, A.G. Fane, Analysis of the effect of turbulence promoters in hollow fiber membrane distillation modules by computational fluid dynamic (CFD) simulations, *J. Membr. Sci.*, 415–416 (2012) 758–769.
- [12] Y.F. Liu, G.H. He, X.D. Liu, G.K. Xiao, B.J. Li, CFD simulations of turbulent flow in baffle-filled membrane tubes, *Sep. Purif. Technol.*, 67 (2009) 14–20.
- [13] G.A. Fimbres-Weihs, D.E. Wiley, Numerical study of mass transfer in three dimensional spacer-filled narrow channels with steady flow, *J. Membr. Sci.*, 306 (2007) 228–243.
- [14] L.J. Xia, A. W.K. Law, A.G. Fane, Hydrodynamic effects of air sparging on hollow fiber membranes in a bubble column reactor, *Water Res.*, 47 (2013) 3762–3772.
- [15] P. L. Clech, V. Chen, T. Fane, Fouling in membrane bioreactors used in wastewater treatment, *J. Membr. Sci.*, 284 (2006) 17–53.
- [16] S. Muthukumar, S. Kentish, S. Lalchandani, M. Ashokkumar, R. Mawson, G.W. Stevens, F. Grieser, The optimisation of ultra-sonic cleaning procedures for dairy fouled ultrafiltration membranes, *Ultrason. Sonochem.*, 12 (2005) 29–35.
- [17] S. Muthukumar, K. Yang, A. Seuren, S. Kentish, M. Ashokkumar, G. Stevens, F. Grieser, The use of ultrasonic cleaning for ultrafiltration membranes in the dairy industry, *Sep. Purif. Technol.*, 39 (2004) 99–107.
- [18] A. Mirzaie, T. Mohammadi, Effect of ultrasonic waves on flux enhancement in microfiltration of milk, *J. Food Eng.*, 108 (2012) 77–86.
- [19] Z. Jalilvand, F.Z. Ashtiani, A. Fouladitajar, H. Rezaei, Computational fluid dynamics modeling and experimental study of continuous and pulsatile flow in flat sheet microfiltration membranes, *J. Membr. Sci.*, 450 (2014) 207–214.
- [20] C. Wilharm, V.G.J. Rodgers, Significance of duration and amplitude in transmembrane pressure pulsed ultrafiltration of binary protein mixtures, *J. Membr. Sci.* 121 (1996) 217–228.
- [21] S. Redkar, V. Kuberbar, R.H. Davis, Modeling of concentration polarization and depolarization with high-frequency back pulsing, *J. Membr. Sci.*, 121 (1996) 229–242.
- [22] M. Gironès i Nogué, I.J. Akbarsyah, L.A.M. Bolhuis-Versteeg, R.G.H. Lammertink, M. Wessling, Vibrating polymeric micro-sieves: Antifouling strategies for microfiltration, *J. Membr. Sci.* 285 (2006) 323–333.
- [23] K.J. Hwang, H.Y. Tsai, S.T. Chen, Enzymatic hydrolysis suspension cross-flow diafiltration using polysulfone hollow fiber module, *J. Membr. Sci.*, 454 (2014) 418–425.
- [24] Y.Y. Liang, M.B. Chapman, G.A. FimbresWeihs, D.E. Wiley, CFD modelling of electro-osmotic permeate flux enhancement on the feed side of a membrane module, *J. Membr. Sci.*, 470 (2014) 378–388.
- [25] Y.L. Li, P.J. Lin, K.L. Tung, CFD analysis of fluid flow through a spacer-filled disk-type membrane module, *Desalination*, 283 (2011) 140–147.
- [26] Y.L. Li, K.L. Tung, Y.S. Chen, K.J. Hwang, CFD analysis of the initial stages of particle deposition in spiral-wound membrane modules, *Desalination*, 287 (2012) 200–208.
- [27] Y. Wang, M. Brannock, S. Cox, G. Leslie, CFD simulations of membrane filtration zone in a submerged hollow fibre membrane bioreactor using a porous media approach, *J. Membr. Sci.*, 363 (2010) 57–66.
- [28] Y.Y. Liang, M.B. Chapman, G.A. FimbresWeihs, D.E. Wiley, CFD modelling of electro-osmotic permeate flux enhancement on the feed side of a membrane module, *J. Membr. Sci.*, 470 (2014) 378–388.
- [29] S. Buethorn, D. Volmering, K. Vossenkaul, T. Wintgens, M. Wessling, T. Melin, CFD simulation of single- and multi-phase flows through submerged membrane units with irregular fiber arrangement, *J. Membr. Sci.*, 384 (2011) 184–197.
- [30] H. Yu, X. Yang, R. Wang, A.G. Fane, Numerical simulation of heat and mass transfer in direct membrane distillation in a hollow fiber module with laminar flow, *J. Membr. Sci.*, 384 (2011) 107–116.
- [31] R. Ghidossi, D. Veyret, P. Moulin, Computational fluid dynamics applied to membranes: state of the art and opportunities, *Chem. Eng. Process*, 45 (2006) 437–454.
- [32] F. Li, W. Meindersma, A.B. de Haan, T. Reith, Optimization of commercial net spacers in spiral wound membrane modules, *J. Membr. Sci.*, 208 (2002) 289–302.
- [33] F. Li, G.W. Meindersma, A.B. de Haan, T. Reith, Optimization of non-woven spacers by CFD and validation by experiments, *Desalination*, 146 (2002) 209–212.
- [34] K. Damak, A. Ayadi, B. Zeghmami, P. Schmitz, A new Navier–Stokes and Darcy’s law combined model for fluid flow in cross-flow filtration tubular membranes, *Desalination*, 161 (2004) 67–77.
- [35] A.L. Ahmad, K.K. Lau, M.Z. Abu Bakar, S.R. Abd.Shukor, Integrated CFD simulation of concentration polarization in narrow membrane channel, *Comput. Chem. Eng.*, 29 (2005) 2087–2095.
- [36] A. Pak, T. Mohammadi, S.M. Hosseinalipour, V. Allahdini, CFD modeling of porous membranes, *Desalination*, 222 (2008) 482–488.
- [37] R.J.G. Lopes, V.S.L. de Sousa, R.M. Quinta-Ferreira, CFD and experimental studies of reactive pulsing flow in environmentally-based trickle-bed reactors, *Chem. Eng. Sci.*, 66 (2011) 3280–3290.
- [38] R. Kaya, G. Deveci, T. Turken, R. Sengur, S. Guclu, D.Y. Koseoglu-Imer, I. Koyuncu, Analysis of wall shear stress on the outside-in type hollow fiber membrane modules by CFD simulation, *Desalination*, 351 (2014) 109–119.
- [39] Y.-L. Li, K.-L. Tung, CFD simulation of fluid flow through spacer-filled membrane module: selecting suitable cell types for periodic boundary conditions, *Desalination*, 233 (2008) 351–358.
- [40] P. Wei, K. Zhang, W. Gao, L.X. Kong, R. Field, CFD modeling of hydrodynamic characteristics of slug bubble flow in a flat sheet membrane bioreactor, *J. Membr. Sci.*, 445 (2013) 15–24.
- [41] Y.F. Liu, G.H. He, B. Li, Z.W. Hu, J. Ju, A comparison of cake properties in traditional and turbulence promoter assisted microfiltration of particulate suspensions, *Water Res.*, 46 (2012) 2535–2544.
- [42] H.G. Goma, R. Sabouni, Energetic consideration and flux characteristics of roughed-surface membrane in presence of reversing shear, *Chem. Eng. Res. Des.*, 92 (2014) 1771–1780.
- [43] K.J. Lee, R.M. Wu, Simulation of resistance of cross-flow microfiltration and force analysis on membrane surface, *Desalination*, 233 (2008) 239–246.